Self-consistent solutions to the intersubband rate equations in quantum cascade lasers: Analysis of a GaAs/$Al_xGa_{1-x}As$ device

K. Donovan,[a] P. Harrison, and R. W. Kelsall
Institute of Microwaves and Photonics, School of Electronic and Electrical Engineering, University of Leeds, Leeds LS2 9JT, United Kingdom

(Received 27 March 2000; accepted for publication 21 November 2000)

The carrier transition rates and subband populations for a GaAs/AlGaAs quantum cascade laser operating in the mid-infrared frequency range are calculated by solving the rate equations describing the electron densities in each subband self-consistently. These calculations are repeated for a range of temperatures from 20 to 300 K. The lifetime of the upper laser level found by this self-consistent method is then used to calculate the gain for this range of temperatures. At a temperature of 77 K, the gain of the laser is found to be 34 $cm^{-1}/(kA/cm^{-2})$, when only electron–longitudinal-optical phonon transitions are considered in the calculation. The calculated gain decreases to 19.6 $cm^{-1}/(kA/cm^{-2})$ when electron–electron transition rates are included, thus showing their importance in physical models of these devices. Further analysis shows that thermionic emission could be occurring in real devices. © *2001 American Institute of Physics.*
[DOI: 10.1063/1.1341216]

I. INTRODUCTION

Quantum cascade lasers have been the focus of much research since they were developed in 1994.[1,2] They have traditionally been based on a InGaAs/AlInAs structure so that the growth could be lattice matched to InP substrates.[3,4] More recent designs have been based on a GaAs/AlGaAs structure, which is a material more commonly used in compound semiconductors.[5] There has been rapid progress in their development and much improvement in their performance.[6,7] At present the only operational quantum cascade lasers are in the mid-infrared frequency range[8,9] but recently models have been proposed which extend the operating frequency into the far-infrared (FIR) range[10] and FIR electroluminescence has been observed in multiple quantum well devices.[11] There are difficulties with FIR intersubband devices, however, because the smaller subband separations required are of the order of the longitudinal optical (LO) phonon energy. This means that detrimental nonradiative transitions are increased, so the quantum efficiency of the device is reduced.[12] Theoretical studies to date have mainly centered around the optimization of the active region structure so that the maximum possible population inversion could be achieved (see for example Refs. 13 and 14). Determination of the population inversion of a device requires calculation of the subband populations and carrier transition rates within the structure.

II. THEORY

A full analysis of a quantum cascade laser requires consideration of not only the active region, where laser emission takes place, but also the injector regions which supply the upper laser level with carriers. The aim of this article is to calculate the populations of the active region and injector subbands in a quantum cascade laser, using a self-consistent approach. The subband populations can then be used to calculate the population ratio and gain of the device.

For a three-level laser, as shown in Fig. 1, ignoring absorption processes, the number of carriers in the second subband is given by

$$\frac{dn_2}{dt} = \frac{n_3}{\tau_{32}} - \frac{n_2}{\tau_{21}}, \tag{1}$$

where $\tau_{32}(\tau_{21})$ represents the average time for an electron in subband 3 (subband 2) to scatter to subband 2 (subband 1). At equillibrium $dn_2/dt = 0$, therefore

$$\frac{n_3}{n_2} = \frac{\tau_{32}}{\tau_{21}}. \tag{2}$$

Hence if $\tau_{32} > \tau_{21}$ then a population inversion would exist between subbands 3 and 2. This has been used to give an indication of the potential for a device to reach a population inversion and works well in, for example, mid-infrared devices where the energy gaps are relatively large and phonon absorption less likely. In later work[13] the energy difference between the lower laser level (subband 2) and the ground state (subband 1) was small and hence backscattering (absorption processes from 1 to 2) were much more significant. To improve the approximation the net rate was used, i.e.,

$$\frac{n_3}{n_2} \sim \frac{\left(\frac{1}{\tau_{21}} - \frac{1}{\tau_{12}}\right)}{\left(\frac{1}{\tau_{32}} - \frac{1}{\tau_{23}}\right)}. \tag{3}$$

However, this is no more than a first order approximation,[10] since the subband populations themselves depend on the intersubband carrier transition rates. This article presents a self-consistent solution of the transition rate equations for a

[a]Author to whom correspondence should be addressed; electronic mail: phykd@sun.leeds.ac.uk

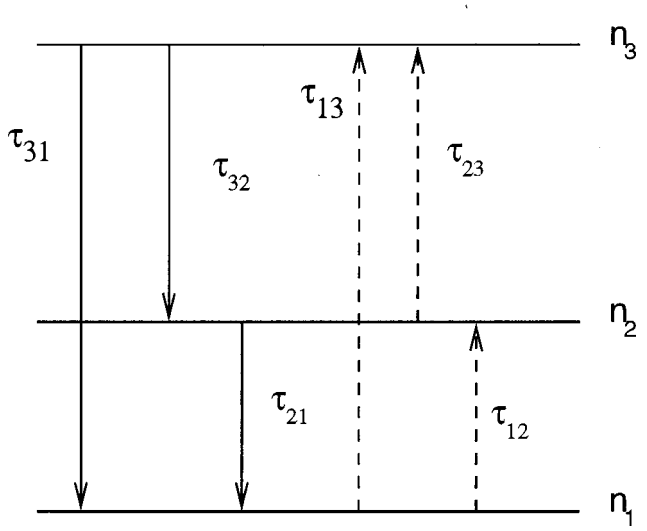

FIG. 1. Energy levels and transition rates in a three-level laser.

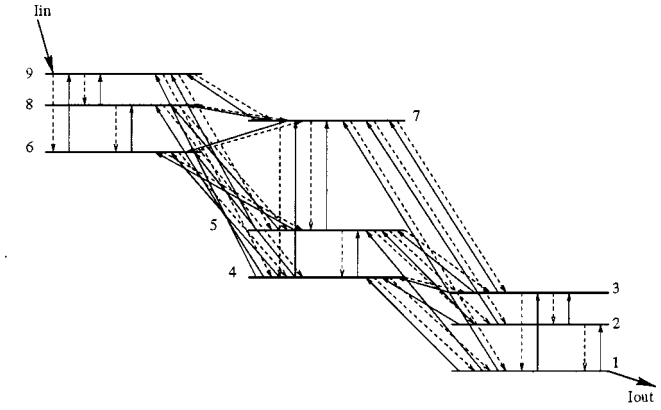

FIG. 3. Carrier transitions in the nine-level system. It was assumed that the upward transitions from levels $|1\rangle$, $|2\rangle$, and $|3\rangle$ into level $|7\rangle$ were negligible, as were the transitions between the injector regions either side of the active region.

working quantum cascade laser.[5] The subband populations and carrier lifetimes were calculated and these were then used to find the gain of the laser.

The energy levels and associated wave functions of the active region and injector were found by numerical solution of the Schrödinger equation[15] for $1\frac{1}{2}$ periods of the superlattice. (One period consists of one injector region and one active region.) A schematic diagram of this nine-level system is shown in Fig. 2. Contrary to the assumption of a miniband in the injector region,[5] there are, in fact, just three energy levels in the injector. Radiative emission is between the third and second energy levels in the active region (called subbands 7 and 5 in the nine-level system). The upper laser level is populated by injection of carriers from the three states 6, 8, and 9, in the left hand injector.

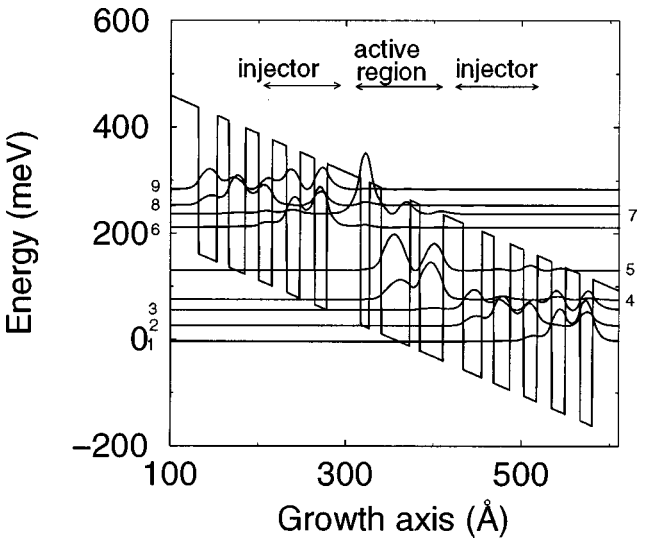

FIG. 2. A schematic diagram of the energy levels and associated wave functions for a mid-infrared quantum cascade laser. The structure studied here consisted of nine energy levels; three injector levels introducing carriers to the active region of the laser, three active region levels, and three injector levels in the next period of the laser, into which carriers are emitted from the active region.

The carrier transitions in the structure are shown in Fig. 3. To simplify the calculation, the assumption was made that subbands 1, 2, and 3 were isolated from 6, 8, and 9; i.e., transition rates between consecutive injector regions were negligible. It was also assumed that upward scattering from subbands 1, 2, and 3 into 7 was negligible. To introduce periodic boundary conditions, the rate equations were written such that carriers were cycled around the nine level system. In a steady state situation, this is equivalent to carriers entering subband 9, the highest injector level, from the previous active region and leaving subband 1, the lowest injector level, to enter the next active region. Given this, the rate equation for subband 1 at equilibrium is given by

$$\frac{dn_1}{dt} = \frac{n_2}{\tau_{21}} + \frac{n_3}{\tau_{31}} + \frac{n_4}{\tau_{41}} + \frac{n_4}{\tau_{46}} + \frac{n_5}{\tau_{51}} + \frac{n_5}{\tau_{56}} + \frac{n_7}{\tau_{71}} + \frac{n_7}{\tau_{76}} - n_1\left(\frac{1}{\tau_{12}} + \frac{1}{\tau_{13}} + \frac{1}{\tau_{14}} + \frac{1}{\tau_{15}} + \frac{1}{\tau_{64}} + \frac{1}{\tau_{65}} + \frac{1}{\tau_{67}}\right) = 0, \tag{4}$$

with the rate equations for subbands 2–9 following similarly. Note that τ_{if} is a function of both n_i and n_f, the initial and final subband populations. This $1\frac{1}{2}$ period model must reflect the full many period system of the true device and hence subband 1 must be equivalent to subband 6. Now backscattering into subband 1 from the next injector cannot be included (because it is outside the $1\frac{1}{2}$ periods considered here), however it is equivalent to the backscattering from the active region subbands 5 and 7 into its equivalent subband 6, hence the inclusion in Eq. (4) of terms like n_5/τ_{56}.

The equations describing the rates dn_1/dt, dn_2/dt, and dn_3/dt are symmetric with those describing dn_6/dt, dn_8/dt, and dn_9/dt. This implies that, when the system has reached a steady state, the number of carriers in subband 6 should equal that in subband 1, so that the injection rates on each side of the active region are equal.

Each rate equation is then rewritten to make a different subband population the subject; i.e., Eq. (4), which describes the number of electrons in subband 1, is rewritten as

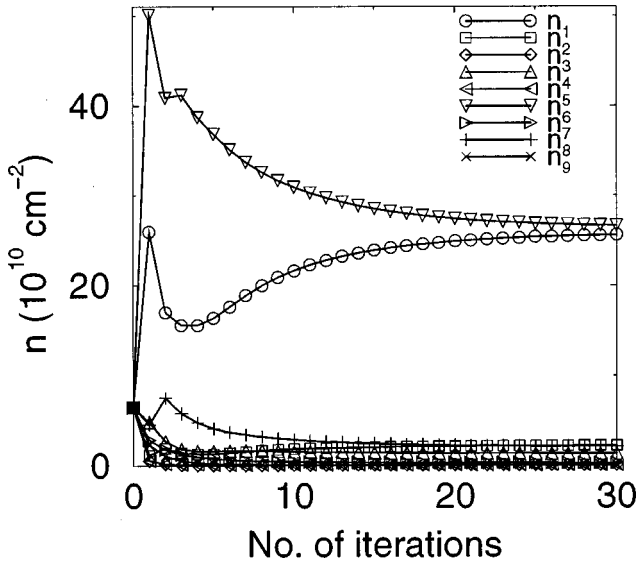

FIG. 4. Subband populations vs the number of iterations of the self-consistent calculation, considering electron–LO phonon scattering only. Convergence is achieved after 20 iterations of the self-consistent calculation, when the gradient of the curve tends to zero. At equilibrium, the corresponding injector levels contain the same number of carriers; i.e., $n_1=n_6$, $n_2=n_8$, and $n_3=n_9$.

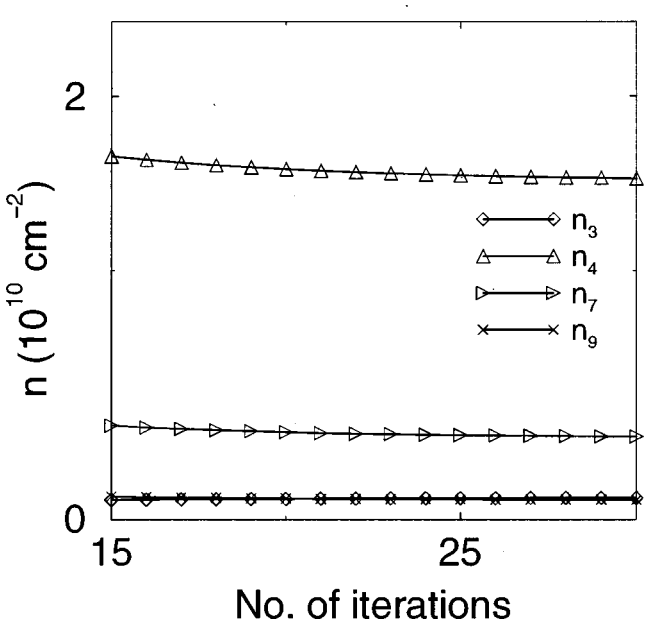

FIG. 5. Subband populations vs the number of iterations of the self-consistent calculation, considering electron–LO phonon scattering only. This figure shows more clearly that $n_3=n_9$.

$$n_1=\frac{\frac{n_2}{\tau_{21}}+\frac{n_3}{\tau_{31}}+\frac{n_4}{\tau_{41}}+\frac{n_5}{\tau_{51}}+\frac{n_7}{\tau_{71}}+\frac{n_4}{\tau_{46}}+\frac{n_5}{\tau_{56}}+\frac{n_7}{\tau_{76}}}{\frac{1}{\tau_{12}}+\frac{1}{\tau_{13}}+\frac{1}{\tau_{14}}+\frac{1}{\tau_{15}}+\frac{1}{\tau_{64}}+\frac{1}{\tau_{65}}+\frac{1}{\tau_{67}}}, \quad (5)$$

with the other eight rate equations producing similar expressions for the subband populations $n_1,n_2,n_3,\ldots..,n_9$. Thus we have a set of equations which specify the population of a subband in terms of the populations of all the other subbands and the scattering rates between them. The problem is to find values for $n_1,n_2,n_3,\ldots..,n_9$ which satisfy all these equations simultaneously.

This is done by assuming equal carrier densities in each subband, calculating the scattering rates and then producing the next best iteration using the series of equations as illustrated by Eq. (5). These new solutions were then renormalized by driving them towards the fixed value for the total carrier density in each quantum well period—deduced from the doping profile ($39\times10^{10}\,\mathrm{cm}^{-2}$). The iteration is continued until self-consistency is achieved; i.e., the values predicted by the series of equations illustrated by Eq. (5) are the same as in the previous evaluation (the method is illustrated in Fig. 4).

The carrier lifetimes in each subband τ_i and the intersubband carrier scattering times τ_{ij} were calculated in the first instance using the electron–LO phonon scattering rates only[15] (to reduce computational time) and then later including electron–electron scattering.[16] Radiative transition rates were calculated using the approach of Smet *et al.*[17]

The gain of a mid-infrared quantum cascade laser can be written as[4]

$$g=\frac{4\pi q}{\epsilon_0 n}\frac{(\tau_{75}-\tau_5)(\tau_7/\tau_{75})}{2\gamma_{75}L_p}\frac{(z_{75})^2}{\lambda}, \quad (6)$$

where q is the electronic charge, n is the refractive index, γ_{75} is the half width half maximum of the luminescence, and L_p is the length of a period. z_{75} is the radiative transition matrix element which can be calculated as[15]

$$(z_{75})^2=\frac{O_{75}\hbar}{2m^*\omega}, \quad (7)$$

where O_{75} is the oscillator strength.

Using this expression, the gain of the device was calculated at a range of temperatures from 20 to 300 K. The lifetimes τ_5, τ_7, and τ_{75} were obtained from the self-consistent solution of the transition rate equations. The values $n=3.2836$, $\gamma_{75}=5.5\,\mathrm{meV}$,[18] $L_p=45.3\,\mathrm{nm}$, and $O_{75}=0.6350\,\mathrm{m}^{-1}\,\mathrm{s}^2$ were used.

III. INCLUSION OF ELECTRON–LO PHONON SCATTERING ONLY

It can be seen in Fig. 4, which shows the subband populations versus the number of iterations at a temperature of 77 K, that the subband populations reach convergence after about 20 iterations of the calculation. At this point $n_1+n_2+n_3+\ldots+n_9=N_{\mathrm{total}}$ and the injector levels to the left and to the right of the active regions have equal populations; i.e., $n_1=n_6$, $n_2=n_8$, and $n_3=n_9$, as can be seen in Fig. 4. See also Fig. 5.

The population ratio n_7/n_5 is shown in Fig. 6. It is a maximum at 120 K but decreases as the temperature is decreased. This can be explained by Fig. 7, which shows that the injection time

$$\tau_{I\mathrm{in}}=\left(\frac{1}{\tau_{67}}+\frac{1}{\tau_{87}}+\frac{1}{\tau_{97}}\right)^{-1}$$

of carriers into the upper laser level is slow at low temperatures and decreases as the temperature rises. The latter is

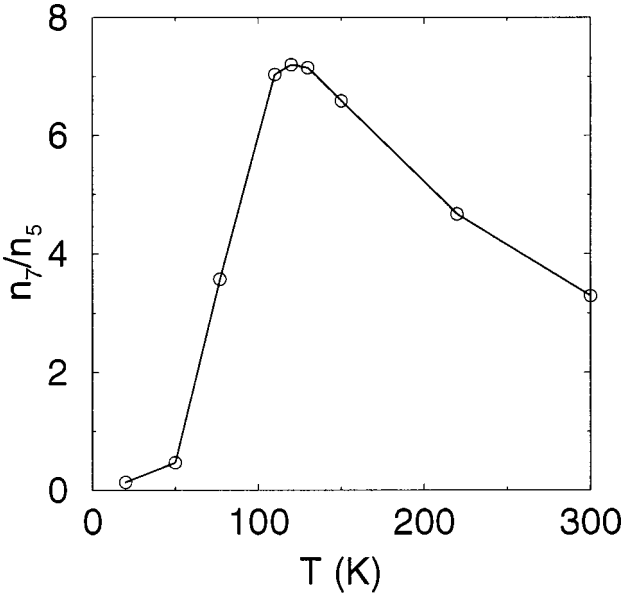

FIG. 6. The population ratio between the upper and lower laser levels vs temperature.

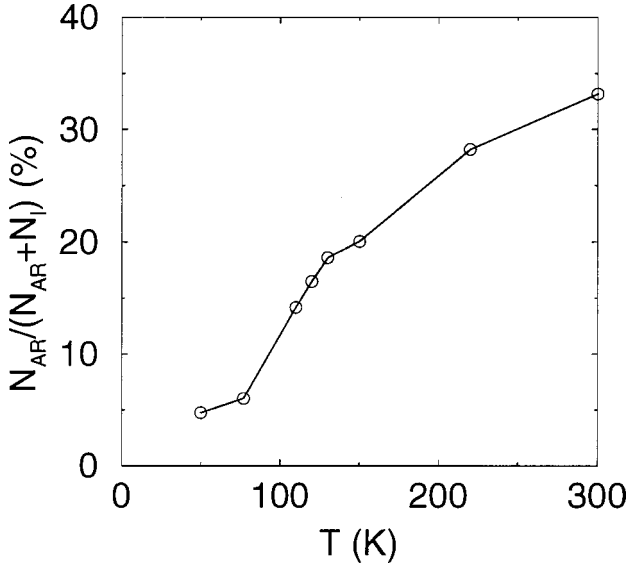

FIG. 8. Percentage of carriers in the active region of the laser as a function of temperature.

because of the thermal broadening of the injector states, in particular the lower energy level $|6\rangle$, and the resulting increased energy overlap. Given that the lifetime for scattering out of the active region into the next injector

$$\tau_{I\text{out}}=\left(\frac{1}{\tau_{53}}+\frac{1}{\tau_{52}}+\frac{1}{\tau_{51}}+\frac{1}{\tau_{43}}+\frac{1}{\tau_{42}}+\frac{1}{\tau_{41}}\right)^{-1}$$

remains almost constant, as illustrated in Fig. 7, then this improving injection rate with temperature results in an increased proportion of the carriers occupying the active region, as illustrated in Fig. 8. As the temperature rises, nonradiative losses from the upper laser level to the lower increase and as usual the population ratio decreases, as illustrated in Fig. 6.

The gain of the laser as a function of temperature is shown in Fig. 9. It is a maximum at low temperatures and has a value of 57 $cm^{-1}/(kA/cm^{-2})$ at 20 K, decreasing to 15 $cm^{-1}/(kA/cm^{-2})$ at 300 K. This is because the nonradiative lifetime of the excited state is higher at low temperatures. The device is quoted as having a maximum operating temperature of 140 K,[5] and at this temperature the gain is 25 $cm^{-1}/(kA/cm^{-2})$. At the working temperature of 77 K, the calculated gain is 34 $cm^{-1}/(kA/cm^{-2})$. This is similar to the value of 30 $cm^{-1}/(kA/cm^{-2})$ calculated in Ref. 10. The gain measured by experiment was found to be 8.7 $cm^{-1}/(kA/cm^{-2})$ at 77 K. This was calculated using G_M

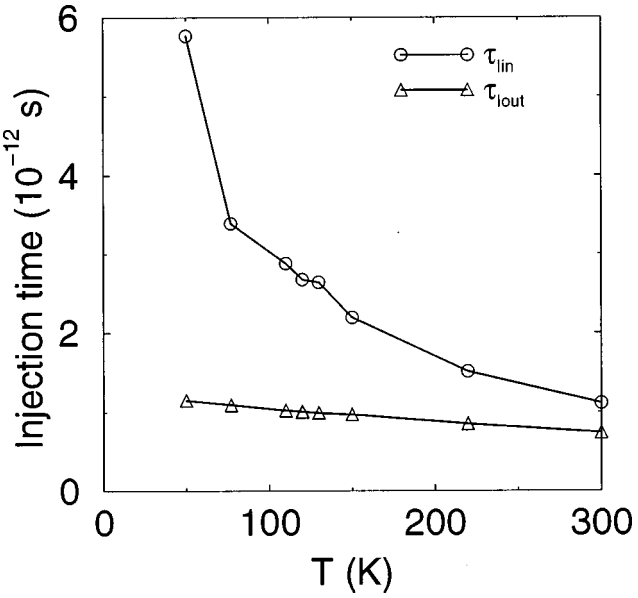

FIG. 7. Injection times $\tau_{I\text{in}}$ and $\tau_{I\text{out}}$ of carriers into and out of the active region, respectively, as a function of temperature.

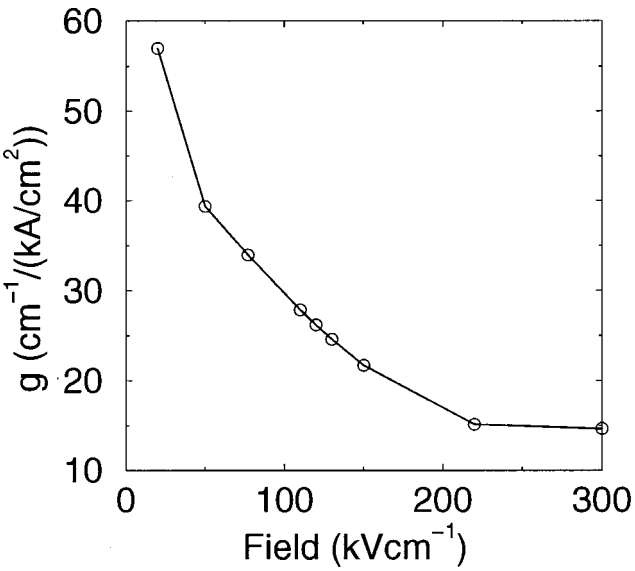

FIG. 9. The gain of the laser vs temperature.

$=gJ_{\mathrm{th}}=(\alpha_M+\alpha_W)/\Gamma$, where G_M is the material gain, J_{th} is the threshold current, and α_M and α_W are the mirror and waveguide losses, respectively.

IV. INCLUSION OF ELECTRON–ELECTRON SCATTERING

At the point of convergence the self-consistent analysis was extended to include calculation of the electron–electron ($e-e$) transition rates. Because the CPU time required to calculate electron–electron scattering is so long, initially these rates were calculated just for those transitions between subbands separated by less than the LO phonon energy; i.e., $2\rightarrow1$, $3\rightarrow2$, $4\rightarrow3$, $7\rightarrow6$, $8\rightarrow7$, and $9\rightarrow8$.

The electron–LO phonon transition rates were calculated, followed by these electron–electron transition rates for a further ten iterations, until convergence was achieved again. The new lifetimes τ_5, τ_7, and τ_{75} were then used to calculate the gain of the device at 77 K. The gain was found to be 23 $\mathrm{cm}^{-1}/(\mathrm{kA/cm}^{-2})$, which is closer to the gain found by experiment. This relatively large change in the calculated gain thus illustrates the importance of electron–electron scattering in these mid-infrared quantum cascade lasers.

All the electron–electron transitions involving subbands 7 and 5 were then included, as it was found from initial calculations that, although the population ratio changed by only 10% upon the inclusion of electron–electron scattering, the lifetimes of 7 and 5 were reduced sufficiently to cause a decrease in the gain of the device. The solution was again iterated to self-consistency.

The gain of the laser was now calculated as 19.6 $\mathrm{cm}^{-1}/(\mathrm{kA/cm}^{-2})$ at 77 K. Because of the extremely long CPU time required, it was not practical to calculate electron–electron scattering rates for all possible transitions in the device. However, the calculations described above have shown that electron–electron scattering is a significant nonradiative loss mechanism, and the inclusion of further electron–electron scattering mechanisms could explain some of the difference between the experimental and calculated gain reported by Sirtori *et al.*[5]

V. THE EFFECT OF ELECTRON TEMPERATURE ON CARRIER TRANSITION RATES

There is some ongoing discussion on the electron temperature within quantum cascade lasers and how this may affect device performance. Elevated electron temperatures can occur as a consequence of short-pulse optical excitation, and pulsed or steady state high field electrical excitation. The device under analysis requires an electric field of 48 $\mathrm{kV\,cm}^{-1}$ for optimum band lineup, which lies well within the range at which electron heating is anticipated.

The electron–LO phonon transition rates for the important transitions $7\rightarrow5$ and $5\rightarrow4$ were calculated for a lattice temperature of 77 K (as used in the experiment)[5] for a range of electron temperatures between 77 and 300 K. The graph of the resulting $e-$LO transition rates against electron temperature is shown in Fig. 10. It can be seen that there is a 3% change in the $e-$LO rate for the $7\rightarrow5$ transition and a 20% change in the $5\rightarrow4$ $e-$LO transition rate. The energy gap between 7 and 5 (ΔE_{75}) is 138 meV, which is greater than the ΔE_{LO}, whereas the $5\rightarrow4$ energy gap is 36.5 meV, which is equal to ΔE_{LO}.

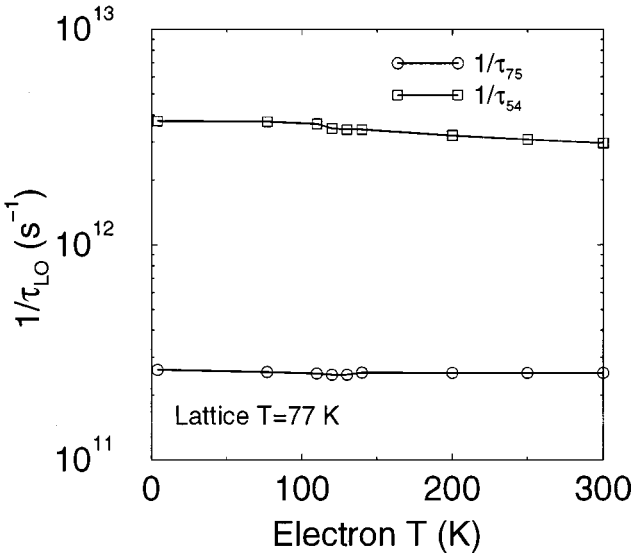

FIG. 10. The electron–LO phonon transition rate as a function of electron temperature. The lattice temperature remained constant at 77 K.

Hence variations in the electron temperature do not change the electron scattering rate significantly in this mid-infrared device. Thus it can be concluded that the electron temperature does not affect the gain directly—although see the discussion in Sec. VI.

VI. OTHER LOSS MECHANISMS

There are two possible loss mechanisms which could explain the difference between the gain calculated theoretically and that obtained by experiment. The first of these is thermionic emission; i.e., the escape of carriers from the upper laser level over the adjacent right hand barrier into the

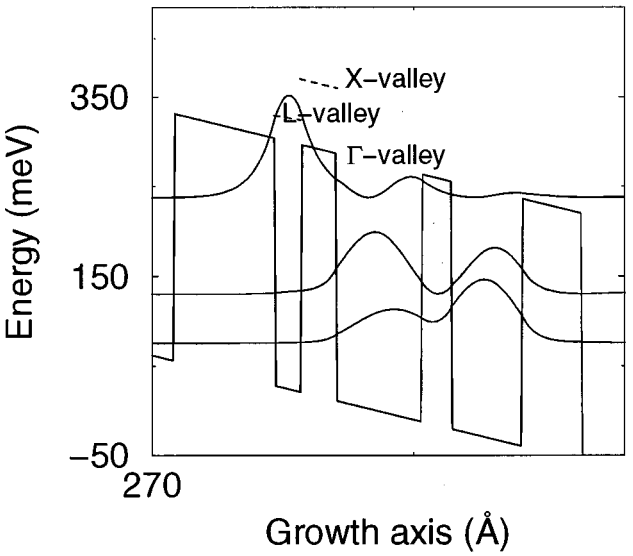

FIG. 11. A schematic diagram of the Γ- and *L* valleys of the GaAs well and the Γ and *X* valleys of the AlGaAs barrier.

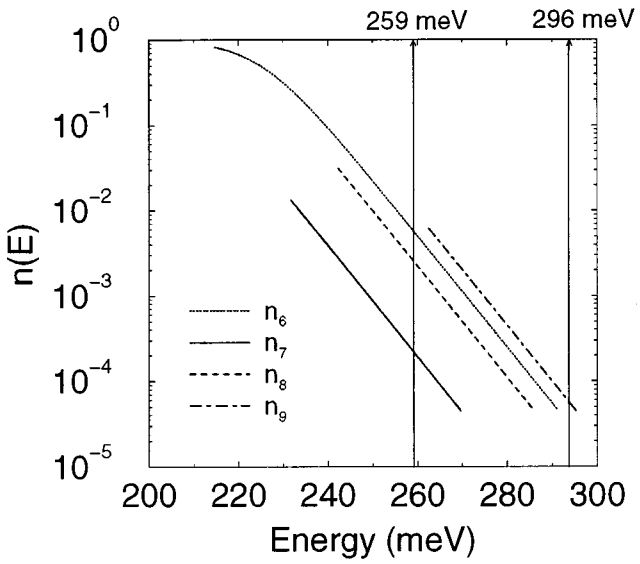

FIG. 12. The quasi Fermi–Dirac distribution of the upper laser level and three highest injector levels at a temperature of 77 K. The absolute energy of the upper laser level $|7\rangle$ is actually above its quasi Fermi energy.

continuum. The energy of the top of the barrier directly adjacent to the well containing the upper laser level, subband 7, is 296 meV. This energy together with the Fermi–Dirac distribution of electron energies of selected states is shown in Fig. 12. There are very few carriers in subband 7 (given by n_7) at or above 296 meV; the subband minimum of subband 7 is 232 meV so carriers would, on average, need to have a kinetic energy of 64 meV to occupy a state near the top of the well. Since $kT = 6.64$ meV at 77 K, it is very unlikely that carriers would be able to undergo thermionic emission from the top of the well. For thermionic emission from the left hand well of the active region to be significant, the electron temperature of the carriers in subband 7 would have to reach 400 K (Fig. 13). There is no evidence to suggest that the

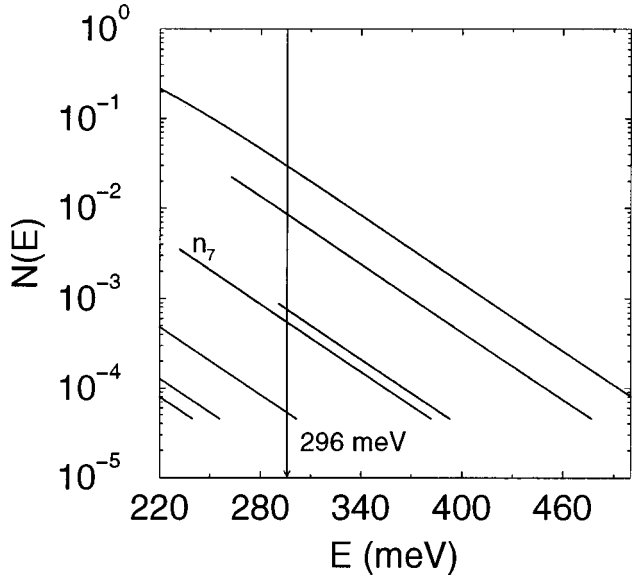

FIG. 13. The quasi Fermi–Dirac distribution at an electron temperature of 400 K.

electron distributions are heated to this extent in quantum cascade lasers operated at 77 K.

However, in Fig. 11 it can be seen that ~10% of the probability distribution of 7 is localized in the central well of the active region. The Fermi energy of 7 is just 44 meV below the top of the central well, which has an absolute energy of 259 meV. About 0.3% of the carriers in 7 are in the central well and at or above this energy (Fig. 11) so is possible that carriers could undergo thermionic emission into the continuum from the upper laser level. As mentioned earlier, an elevated electron temperature, while not affecting the gain directly, would give an increased loss in this manner, thus lowering the gain. This could be one reason why the measured gain is below that calculated here.

Another loss process that has been suggested is intervalley scattering.[5] The intervalley scattering process with the lowest energy threshold in this system is the $\Gamma - L$ transfer in the GaAs quantum well. However, the $\Gamma - L$ energy separation is ~330 meV, which is above the Γ point in the barrier just discussed, so intervalley transfer is unlikely, unless the electron temperature is considerably higher than the lattice temperature.

VII. CONCLUSIONS

A self-consistent analysis of the transition rate equations for a mid-infrared quantum cascade laser has been used to calculate the subband populations and transition rates for a nine-level system consisting of two injectors and an active region. Calculations show that a population ratio greater than 3 may be expected at 77 K. It was found that electron–electron scattering must be included in the calculation of laser gain, to avoid substantial overestimation of this parameter. Further reductions in gain are most likely due to thermionic emission from the active region into continuum states.[19]

ACKNOWLEDGMENTS

The authors would like to thank the School of Electronic and Electrical Engineering and the University of Leeds for financial support.

[1] J. Faist, F. Capasso, D. L. Sivco, C. Sirtori, A. L. Hutchinson, and A. Y. Cho, Science **264**, 553 (1994).
[2] J. Faist, F. Capasso, D. L. Sivco, C. Sirtori, A. L. Hutchinson, and A. Y. Cho, Electron. Lett. **30**, 865 (1994).
[3] J. Faist, F. Capasso, C. Sirtori, D. L. Sivco, A. L. Hutchinson, and A. Y. Cho, Appl. Phys. Lett. **66**, 538 (1995).
[4] C. Sirtori, J. Faist, F. Capasso, D. L. Sivco, A. L. Hutchinson, S. N. G. Chu, and A. Y. Cho, Appl. Phys. Lett. **68**, 1745 (1996).
[5] C. Sirtori, P. Kruck, S. Barbieri, P. Collot, J. Nagle, M. Beck, J. Faist, and U. Oesterle, Appl. Phys. Lett. **73**, 3486 (1998).
[6] J. Faist, F. Capasso, C. Sirtori, D. L. Sivco, A. L. Hutchinson, and A. Y. Cho, Appl. Phys. Lett. **67**, 3057 (1995).
[7] C. Sirtori, J. Faist, F. Capasso, D. L. Sivco, A. L. Hutchinson, and A. Y. Cho, Appl. Phys. Lett. **69**, 2810 (1996).
[8] D. Hofstetter, J. Faist, M. Beck, and U. Oesterle, Appl. Phys. Lett. **75**, 3769 (1999).
[9] A. Müller, M. Beck, J. Faist, U. Oesterle, and M. Ilegems, Appl. Phys. Lett. **75**, 1509 (1999).
[10] K. Donovan, P. Harrison, R. W. Kelsall, and P. Kinsler, IEEE 6th International Conference on Terahertz Electronics Proceedings, 1998, p. 223.

[11] M. Rochat, J. Faist, M. Beck, U. Oesterle, and M. Ilegems, Appl. Phys. Lett. **73**, 3724 (1998).
[12] I. Lyubomisrky, Q. Hu, and M. R. Melloch, Appl. Phys. Lett. **73**, 3043 (1998).
[13] K. Donovan, P. Harrison, R. W. Kelsall, and P. Kinsler, Superlattices Microstruct. **25**, 373 (1999).
[14] P. Harrison and R. W. Kelsall, J. Appl. Phys. **81**, 7135 (1997).
[15] P. Harrison, *Quantum Wells, Wires and Dots* (Wiley, Chichester, 1999).
[16] P. Kinsler, P. Harrison, and R. W. Kelsall, Phys. Rev. B **58**, 4771 (1998).
[17] J. H. Smet, C. G. Fonstad, and Q. Hu, J. Appl. Phys. **79**, 9305 (1996).
[18] C. Sirtori (private communication).
[19] P. Harrison, Appl. Phys. Lett. **75**, 2800 (1999).